Demystifying the Origin of Vibrational Coherence Transfer Between the S_1 and T_1 States of the Pt-pop Complex

Pijush Karak,[†] Kenneth Ruud,[*,‡] and Swapan Chakrabarti[*,†]

†*Department of Chemistry, University of Calcutta, 92 A. P. C. Road, Kolkata – 700009, West Bengal, India.*

‡*Hylleraas Centre for Quantum Molecular Sciences, Department of Chemistry, University of Tromsø – The Arctic University of Norway, 9037 Tromsø, Norway.*

E-mail: kenneth.ruud@uit.no; swcchem@caluniv.ac.in

Abstract

We demonstrate that spin-vibronic coupling is the most significant mechanism in vibrational coherence transfer(VCT) from the singlet(S_1) to the triplet(T_1) state of the $[Pt_2(P_2O_5H_2)_4]^{4-}$ complex. Our time-dependent correlation function-based study shows that the rate of intersystem crossing (k_{ISC}) through direct spin-orbit coupling is negligibly small, making VCT vanishingly small due to the ultrashort decoherence time(2.5 ps). However, the inclusion of the spin-vibronic contribution to the net k_{ISC} in selective normal modes along the Pt-Pt axis increases the k_{ISC} to such an extent that VCT becomes feasible. Our results suggest that k_{ISC} for the $S_1 \rightarrow T_2$(τ_{ISC} =1.084 ps) is much faster than the $S_1 \rightarrow T_1$(τ_{ISC} =763.4 ps) and $S_1 \rightarrow T_3$(τ_{ISC} =13.38 ps) in CH_3CN solvent, indicating that VCT is possible from the low-lying excited singlet (S_1) to the triplet(T_1) state through the intermediate T_2 state. This is the first example where VCT occurs solely due to spin-vibronic interactions. This finding can pave the way for new types of photo-catalysis.

Graphical TOC Entry

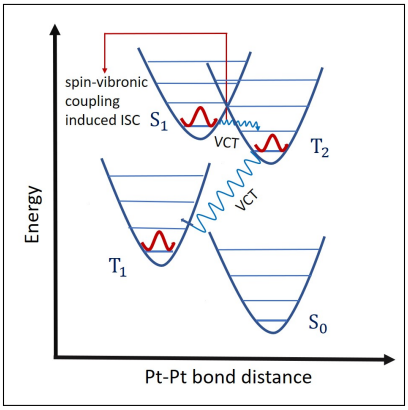

With the advent of highly sophisticated spectroscopic tools, it has become possible to explore details of the mechanisms that determine the efficiency of certain photo-physical processes occurring in the excited state, such as energy and electron transfer in natural and artificial light-harvesting systems. Such detailed insight requires going beyond a pure-state quantum mechanical formalism.[1] The wave-like features of such transfer processes suggests that quantum coherence—in other words, the off-diagonal matrix elements of the density operator—plays an important role at ultrashort time scales.[2–5] However, it has also been found that whereas electronic coherence exists only for a few femtoseconds, the vibrational coherence(VC) can persist up to several picoseconds and it is therefore much easier to probe VC and its transfer from one electronic state to the other, providing us with a better understanding of the these processes.[6] In the recent past, the bimetallic Pt complex $[Pt_2(P_2O_5H_2)_4]^{4-}$, aka Pt-pop, has received significant attention as an interesting transition metal complex[7–11] due to the experimental realization of vibrational coherence transfer(VCT)[12,13] during intersystem(ISC) crossing.[13–19] To gain insight into the origin of this phenomenon, the structures of the excited states of the Pt-pop complex have been investigated using different experimental techniques[20–27] as well as various computational electronic structure methods.[18,28–30] It has been argued that, in order to conserve the vibrational coherence between the low-lying excited singlet and triplet states, the ISC rate should be much faster than the rate of decoherence of the vibrational wave packet formed in the first excited singlet state.

Recently, Monni et al.[13] have revisited the problem of VCT in the Pt-pop complex using 2D UV transient absorption(TA) spectroscopy in combination with QM/MM molecular dynamics simulations. They found that strong solvent-dependent ultrafast ISC is responsible for VCT from the low-lying excited singlet to triplet states. They proposed that the higher-lying triplet state(T_2) is energetically similar to the S_1 state due to its stabilization in polar acetonitrile solvent, which leads to an ultrafast ISC(τ_{ISC}=0.7 ps)-guided VCT from the S_1 to T_1 state. van der Veen et al.[17] have previously observed such ultrafast ISC between the S_1 and T_1 states in other solvents than acetonitrile using time-resolved femtosecond polychromatic

fluorescence up-conversion and femtosecond broadband transient absorption spectroscopy. They also reported that the vibrational wave packet formed in the S_1 state upon excitation is conserved in that state during the vibrational relaxation time, but their investigation did not consider the transfer of vibrational coherence from the S_1 to the T_1 state. Further it was argued that, due to the D_{4h} symmetry of the Pt-pop complex, the spin-orbit coupling matrix elements (SOCME) between the singlet and the triplet manifolds should in principle be small, and preventing ultrafast ISC even if the energy gap between the solvent-stabilized singlet and the triplet states is sufficiently low.[17,31]

To unravel the origin of the ultrafast ISC-driven VCT in the Pt-pop complex, we here go beyond the Franck–Condon regime, adopting a time-dependent correlation function (TDCF)-based method[32–36] with explicit inclusion of spin-vibronic coupling[37–40] to calculate the different pathways contributing to k_{ISC} in the Pt-pop complex. We also investigate the effect of the solvent on k_{ISC}.

The optimized ground-state geometry of the Pt-pop complex is shown in Figure 1. The

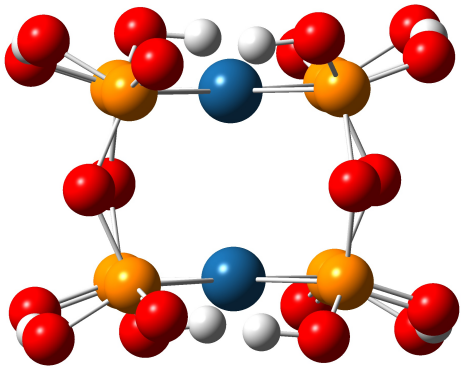

Figure 1: Optimized ground-state geometry of the $[Pt_2(P_2O_5H_2)_4]^{4-}$ complex. Here blue, red, orange and white colors indicates the Pt, O, P and H atoms, respectively.

gas phase- and solvent-optimized geometries of the ground (S_0) and excited states (S_1, T_1, T_2

and T_3) of the Pt-pop complex have been performed using GAUSSIAN 16[41] with the B3LYP exchange-correlation functional.[42–44] In our calculations, we have used the 6-311G+(d,p) basis set[45,46] for P, O and H and the effective core potential(ECP) corrected LANL2DZ basis[47] for Pt. Norman and Jensen[48] have shown that the structural parameters of an organometallic Pt-complex were hardly affected when ECPs were employed only for Pt as compared to using ECPs both for Pt and P. Moreover, they found that the change in the Pt-C bond length of their studied complex as obtained with ECPs and with all-electron four-component relativistic calculations is negligible, indicating that the use of ECP for Pt is sufficient for the geometry optimization of the Pt-pop complex. The excited-state geometry optimizations have been carried out using time-dependent density functional theory(TDDFT). A discussion of the different optimized structures can be found in the Supporting Information(SI). To test the sensitivity of our results on the computational model, we have considered two additional functionals, namely, HSE06[49] and PBE0.[50] The corresponding results are collected in the supporting information. We have found that the geometric parameters, and absorption and emission wavelengths obtained from TDDFT/B3LYP, are comparable to the HSE06 and PBE0 results. The SOCME calculations have been performed with ORCA[51,52] using CASSCF(16e,12o)/NEVPT2[53] in combination with the def2-TZVP basis. The RIJK two-electron integral approximation with a decontracted def2/JK basis[54] has been used to reduce the computational cost of the calculations.

To explain the observed VCT between the S_1 and T_1 electronic states through intersystem crossing, we have calculated k_{ISC} for both the $S_1 \rightarrow T_1$, $S_1 \rightarrow T_2$ and $S_1 \rightarrow T_3$ pathways using Fermi's Golden rule to first order in perturbation theory. Etinski, Tatchen and Marian[33] have derived three distinct formulas for the evaluation of the intersystem crossing rate constant(k_{ISC}). Recently, Karak and Chakrabarti[55] simplified their TDCF method considering only the direct SOC in the evaluation of k_{ISC}. However, it is worth noting that if the direct SOC between the singlet and the triplet states is very small, it is necessary to

go beyond the Franck-Condon regime, i.e. to include spin-vibronic contributions to the ISC rate in order to obtain meaningful results. In the present context, the total k_{ISC} is therefore expressed as

$$k_{ISC} = k_{ISC}^{DSO} + k_{ISC}^{SV}, \tag{1}$$

where k_{ISC}^{DSO} describes the ISC rate constant involving the direct spin-orbit(DSO) coupling mechanism, and k_{ISC}^{SV} represents the additional contribution that comes from spin-vibronic(SV) interactions. The expressions for both k_{ISC}^{DSO} and k_{ISC}^{SV} at finite temperatures as derived by Etinski, Rai-Constapel and Marian[38] are given as

$$\begin{aligned} k_{ISC}^{DSO} = & \frac{1}{Z}|\langle S|\hat{H}_{SO}|T\rangle|^2 \\ & \times \int_{-\infty}^{\infty} \sqrt{\frac{det(\mathbf{S_S^{-1}S_T^{-1}\Omega_S\Omega_T})}{det(\mathbf{J^\dagger\Omega_T B_T J + \Omega_S B_S})det(\mathbf{J^\dagger\Omega_T B_T^{-1} J + \Omega_S B_S^{-1}})}} \\ & \times \exp\left[\mathbf{D}^\dagger\left(\mathbf{\Omega_T B_T J(J^\dagger\Omega_T B_T J + \Omega_S B_S)^{-1} J^\dagger\Omega_T B_T - \Omega_T B_T}\right)\mathbf{D}\right] \times e^{it\Delta E_{ST}}dt, \end{aligned} \tag{2}$$

and,

$$\begin{aligned} k_{ISC}^{SV} = & \frac{1}{Z}\int_{-\infty}^{\infty} \sqrt{\frac{det(\mathbf{S_S^{-1}S_T^{-1}\Omega_S\Omega_T})}{det(\mathbf{J^\dagger\Omega_T B_T J + \Omega_S B_S})det(\mathbf{J^\dagger\Omega_T B_T^{-1} J + \Omega_S B_S^{-1}})}} \\ & \times \exp\left[\mathbf{D}^\dagger\left(\mathbf{\Omega_T B_T J(J^\dagger\Omega_T B_T J + \Omega_S B_S)^{-1} J^\dagger\Omega_T B_T - \Omega_T B_T}\right)\mathbf{D}\right] \\ & \times \left(\left(\mathbf{D^\dagger\Omega_T B_T J(J^\dagger\Omega_T B_T J + \Omega_S B_S)^{-1} C(J^\dagger\Omega_T B_T J + \Omega_S B_S)^{-1} J^\dagger\Omega_T B_T D}\right)\right. \\ & \left. + \frac{1}{2}Tr(\mathbf{C(J^\dagger\Omega_T B_T J + \Omega_S B_S)^{-1}}) - \frac{1}{2}Tr(\mathbf{C(J^\dagger\Omega_T B_T{}^{-1} J + \Omega_S B_S{}^{-1})^{-1}})\right) \times e^{it\Delta E_{ST}}dt. \end{aligned} \tag{3}$$

In the above equations, $\mathbf{\Omega}$, $\mathbf{B}$, $\mathbf{S}$ and $\mathbf{C}$ are defined as $(\mathbf{\Omega_S})_{ii} = (\omega_S)_i$, $(\mathbf{\Omega_T})_{ii} = (\omega_T)_i$, $(\mathbf{B_T})_{ii} = \tanh(\frac{(\omega_T)_i t}{2})$, $(\mathbf{B_S})_{ii} = \tanh(\frac{i(\beta - it)\omega_{Si})}{2})$, $(\mathbf{S_T})_{ii} = \sinh(i(\omega_T)_i t)$, $(\mathbf{S_S})_{ii} = \sinh((\beta - it)\omega_{Si}))$, $\mathbf{C} = \mathbf{b_i b_j}^\dagger$, where ω_{Si} and ω_{Ti} are the frequencies of the i-th mode of the singlet and the triplet states, respectively, and $\mathbf{b}$ is a column vector known as the first-order derivative

coupling term. The expression for $\mathbf{b}$ is

$$\mathbf{b} = \frac{\partial \langle \mathrm{S}|\hat{H}_{\mathrm{so}}|\mathrm{T}\rangle}{\partial \mathbf{Q}}\bigg|_{\mathbf{q_0}}, \tag{4}$$

where $\mathbf{Q}$ denotes the dimensionless normal coordinates and $\mathbf{q_0}$ is the coordinate of the equilibrium geometry of the initial state. In addition, $\mathbf{J}$ and $\mathbf{D}$ indicate the Duschinsky rotation matrix[55–58] and displacement vector, respectively, which are connected through the relation $\mathbf{Q_T} = \mathbf{J}\mathbf{Q_S} + \mathbf{D}$, where $\mathbf{Q_S}$ and $\mathbf{Q_T}$ are the dimensionless normal coordinates of the singlet and triplet electronic states, respectively. $Z = \sum_i e^{-\beta E_i}$ is the vibrational partition function of the initial electronic state and $\beta = \frac{1}{kT}$, where E_i, T and k represent the energy of the i'th vibrational level, temperature and Boltzmann constant, respectively. In both eqs 2 and 3, the energy gap between the singlet(S) and the triplet(T) states is denoted by ΔE_{ST}.

In our present approach, after separating eqs 2 and 3 into real and imaginary parts, we have considered only the real part for the calculation of $\mathrm{k_{ISC}}$ since the imaginary part is an odd function of time. The separation of the $\mathrm{k_{ISC}^{DSO}}$ part at the finite temperature region has already been presented by Karak and Chakrabarti,[55] whereas the details of the simplified equation we arrive at after separation of $\mathrm{k_{ISC}^{SV}}$ is provided in the Supporting Information. Moreover, the derivative coupling term is evaluated numerically using a finite vector differentiation technique, the corresponding formula given as

$$\frac{\partial}{\partial \mathbf{Q}} \mathrm{SOC}\big|_{\mathbf{q_0}} = \frac{\mathrm{SOC}\big|_{\mathbf{q_0}+\delta} - \mathrm{SOC}\big|_{\mathbf{q_0}-\delta}}{2\delta} \tag{5}$$

In the above equation, $\mathbf{Q}$ represents dimensionless coordinates of the respective normal mode and δ denotes the displacement from the equilibrium geometry($\mathbf{q_0}$) along a particular direction of $\mathbf{Q}$. Here the displacement is chosen as 0.1. The SOCMEs corresponding to these two modified geometries are then computed, using eq 5 to evaluate the derivative coupling term. The calculated SOCME and the energy gaps between the $\mathrm{S_1 - T_1}$, $\mathrm{S_1 - T_2}$

and $S_1 - T_3$ states both in the gas and solvent phases are given in Table 1.

Table 1: Spin-Orbit Coupling in cm^{-1} and energy gap in eV as obtained from CASSCF(16e,12o)/NEVPT2 method.

Transition	Direct SOC/gas	Direct SOC/CH_3CN	ΔE/gas	ΔE/CH_3CN
$S_1 \rightarrow T_1$	0.022	0.01	1.1405	1.2061
$S_1 \rightarrow T_2$	0.6284	0.00	0.158	0.184
$S_1 \rightarrow T_3$	0.092	0.02	-0.077	0.078

The data in Table 1 clearly show that the direct SOC between S_1-T_1, S_1-T_2 and S_1-T_3 are very small both in gas phase and in CH_3CN solvent. These observations can be qualitatively understood by examining the natural transition orbitals(NTOs) for the hole state of S_1 and particle states of T_1, T_2 and T_3 in CH_3CN, as shown in Figure 2. We see that the hole state of S_1 has a dominant $d_{z^2}\sigma^*$ character that comes from the Pt-Pt bond, whereas the particle state of T_1 is of more $p\sigma$ type, and as a consequence the SOC between S_1-T_1 should be insignificant[59] since neither the L_z nor the L_+/L_- operators can connect these two states and their small value only suggests that the mixing of orbitals leads to a slight relaxation of the conservation of the z-component of the total angular momentum. In the gas phase, the major contribution to the particle state of T_2 comes from the d_{xy} orbital of Pt. In this case too, $\langle d_{z^2}|L_-|d_{xy}\rangle$ vanishes[59] and the small SOC arises primarily because these d-orbitals are no longer pure orbitals. However, the situation changes dramatically in the presence of CH_3CN, where the particle state of T_2 regains $p\sigma^*$ character in addition to a small d_{xy} contribution, making the direct SOC of S_1-T_2 in this case virtually zero. The nature of the particle state of T_3 is similar to that of T_2 and as a consequence, the SOCME between S_1 and T_3 should also be small. The NTOs for the gas phase are collected in the Supporting Information. We see from Table 1 that CH_3CN plays a significant role in stabilizing the T_3 state. In particular, the interaction between the polar CH_3CN solvent and Pt-pop in the T_3 state pushes its energy level below that of S_1. It is important to mention here that although Monni et al.[13] has probed solvent stabilization of the T_2 state, the corresponding stabilization of the T_3 state has not yet been explored experimentally. These results demonstrate

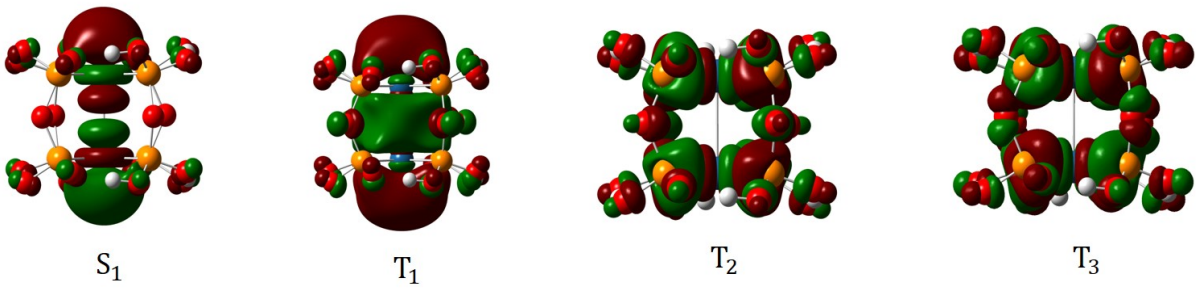

Figure 2: Natural transition orbitals(NTO) of Pt-pop complex for the S_1(hole), T_1(particle), T_2(particle) and T_3(particle) states with isovalue = 0.02.

that the ultrafast ISC-guided transfer of vibrational coherence from S_1 to T_1 is not feasible, and that it is necessary to explore the role of spin-vibronic contributions to the net k_{ISC} value.

It is well established at the experimental level[12,13,17] that VCT in the Pt-pop complex involves the Pt-Pt bond. Keeping this fact in mind, we have computed the derivative coupling term of the SOC considering only two normal modes of the initial electronic state(S_1) in CH_3CN solvent, where one normal mode exhibits symmetric(ν = 121 cm^{-1}) and the other antisymmetric stretching(ν = 153 cm^{-1}) along the Pt-Pt axis. Table 2 collects the calculated derivative spin-orbit coupling term, and the corresponding normal mode displacement vectors in CH_3CN solvent are shown in Figure 3. Displacement vectors involving the Pt-Pt bond in the gas phase are provided in the Supporting Information.

We have used our in-house developed TDCF code to calculate the real part of k_{ISC} for the Pt-pop complex both in solvent and gas phase at a temperature of 300K, both with and without spin-vibronic coupling. The rate constants obtained with both the direct SOC(k_{ISC}^{DSO}) and due to the spin-vibronic coupling(k_{ISC}^{SV}) are presented in Table 3. In order to ensure convergence of the numerical integration of eqs 2 and 3, we have used a Gaussian damping function so that the real part of the TDCF decays within some selected time interval that ensures the incorporation of the effect of all vibrational modes in the evaluation of k_{ISC}. All

Table 2: Derivative Spin-Orbit Coupling as obtained from CASSCF(16e,12o)/NEVPT2 computation with def2-TZVP basis set. ν is the frequency of the normal mode.

Medium	Transition	#Normal mode	ν (cm^{-1})	$\frac{\partial SOC}{\partial q}$($cm^{-1}$)
Gas	$S_1 \rightarrow T_1$	9	136.23	0.15
	$S_1 \rightarrow T_2$			8.55
	$S_1 \rightarrow T_3$			0.39
Gas	$S_1 \rightarrow T_1$	10	136.28	0.05
	$S_1 \rightarrow T_2$			0.07
	$S_1 \rightarrow T_3$			0.00
Solvent(CH_3CN)	$S_1 \rightarrow T_1$	9	121.24	1.90
	$S_1 \rightarrow T_2$			14.29
	$S_1 \rightarrow T_3$			6.90
Solvent(CH_3CN)	$S_1 \rightarrow T_1$	13	153.43	0.14
	$S_1 \rightarrow T_2$			9.65
	$S_1 \rightarrow T_3$			0.16

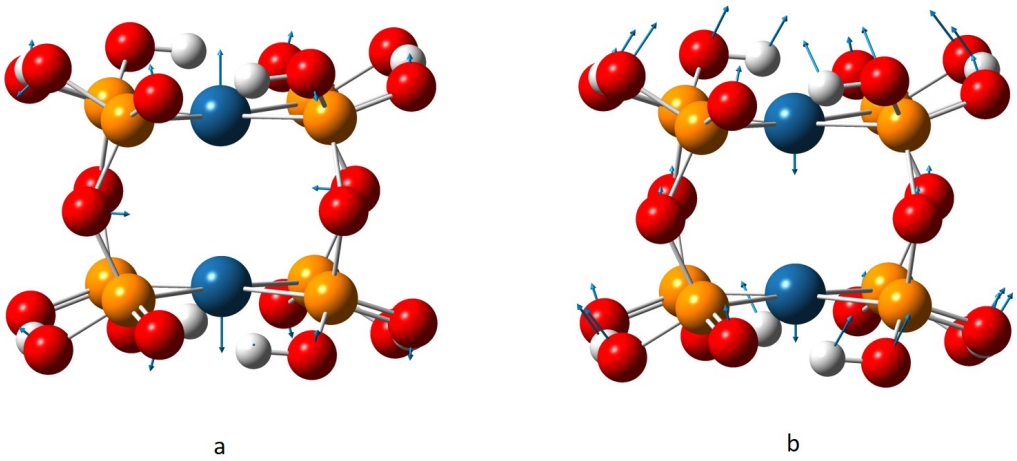

Figure 3: Normal mode displacement vectors along the Pt-Pt axis with (a) symmetric stretching($\nu = 121 cm^{-1}$) and (b) antisymmetric stretching($\nu = 153 cm^{-1}$)

the rate constant calculations are done with a damping parameter of 2.0 cm^{-1} and the nature of the damping of the real part of the TDCF is presented in the supporting information. The physical significance of the damping factor has been discussed elsewhere.[38] We note that there are no experimental results for k_{ISC} of the Pt-pop complex available in the gas phase. However, in order to have a better understanding of the physical origin of the ultrafast ISC, we have repeated all calculations on the gas-phase geometry of the Pt-pop complex. As

Table 3: The computed k_{ISC} (s^{-1}) with both the direct spin-orbit and spin-vibronic coupling in the solvent and the gas phases at 300K. Here the number of intervals used for the integration is 20000 and the upper limit of time is set to 10 ps with damping parameter = 2.0 cm^{-1}.

Transition	Medium	k_{ISC}^{DSO}	k_{ISC}^{SV}
$S_1 \rightarrow T_1$	Gas	3.76×10^{03}	5.29×10^{08}
$S_1 \rightarrow T_2$		2.97×10^{06}	1.40×10^{12}
$S_1 \rightarrow T_3$		7.10×10^{01}	1.15×10^{06}
$S_1 \rightarrow T_1$	Solvent(CH_3CN)	1.09×10^{02}	1.31×10^{09}
$S_1 \rightarrow T_2$		-	9.22×10^{11}
$S_1 \rightarrow T_3$		1.96×10^{03}	7.47×10^{10}

discussed earlier, the T_3 state lies above the S_1 state in the gas phase and it is very unlikely to observe an up-hill ISC between $S_1 \rightarrow T_3$. However, the thermal energy helps promote the ISC between these states with relatively higher SOC values in comparison to that of $S_1 \rightarrow T_1$. In general, Table 3 suggests that spin-vibronic coupling has a strong influence on the rate of ISC and this is true for both the gas and solvent phases and more importantly, spin-vibronic coupling has the highest impact on the k_{ISC} value associated with $S_1 \rightarrow T_2$ pathway in the solvent, which otherwise has no detectable rate constant of ISC when only considering direct SOC. In CH_3CN, the computed k_{ISC}^{SV} for $S_1 \rightarrow T_1$ and $S_1 \rightarrow T_3$ are found to be 1.31×10^{09} s^{-1} and 7.47×10^{10} s^{-1}, respectively and the corresponding rate constant for the $S_1 \rightarrow T_2$ pathway is 9.22×10^{11} s^{-1}, indicating that $S_1 \rightarrow T_2$ is the major ISC pathway in CH_3CN. In order to check the role of the other normal modes on the spin-vibronic interaction and the net k_{ISC} value, we have considered four additional normal modes where the motion of Pt atoms are involved together with the ligand moieties. The magnitude of the derivative coupling term as well as the rate of ISC for these additional normal modes are supplied in Table S3 of the supporting information(SI). With the inclusion of these additional modes, the net k_{ISC} values for the $S_1 \rightarrow T_1$, $S_1 \rightarrow T_2$ and $S_1 \rightarrow T_3$ channels change to 1.88×10^{09} s^{-1}, 1.04×10^{12} s^{-1} and 1.42×10^{11} s^{-1}, respectively, which further strengthens our argument that spin-vibronic interaction is dominant only in the Pt-Pt stretching modes.

Although the spin-vibronic coupling changes the overall rate constant of the ISC significantly, it is still insufficient for directly transferring the vibrational coherence from S_1 to T_1 because the time (τ_{ISC}=763.4 ps) required to realize ISC between these two states is much larger than the experimental decoherence time (τ=2.5 ps).[12,13,17] In contrast, the calculated k_{ISC}^{SV} values for $S_1 \rightarrow T_2$ and $S_1 \rightarrow T_3$ in CH_3CN solvent demonstrate that ISC in these two channels will take place at a time scale of τ_{ISC}=1.084 ps and τ_{ISC}=13.38 ps, respectively, and these results decisively indicate that VCT will occur only in the $S_1 \rightarrow T_2$ channel. We note that the experimental[13] τ_{ISC} value for $S_1 \rightarrow T_2$ in CH_3CN has been found to be 0.7 ps, which is bit smaller than the theoretically predicted value. Nonetheless, the overall theoretical results are in good agreement with available experimental results and give us a clear indication that strong spin-vibronic coupling induced ultrafast ISC helps facilitate VCT through an indirect $S_1 \rightarrow T_2 \rightarrow T_1$ pathway.

To summarize, we have shown that the vibrational coherence from S_1 to T_1 in the Pt-pop complex is feasible in CH_3CN solvent due to ultrafast ISC between S_1 and T_2. We have considered two particular normal modes, namely the symmetric and antisymmetric stretching along the Pt-Pt axis of the complex, and have evaluated the first-order derivative coupling term with respect to spin–orbit coupling and computed the rate constants of ISC using the real part of the time-dependent correlation function. Our analysis suggests that the first-order spin-vibronic coupling term enhances the rate constant of ISC for the $S_1 \rightarrow T_2$ pathway to such an extent that the time required for ISC along this pathway is shorter than the decoherence time of the vibrational wave packet, eventually leading to VCT between S_1 to T_1 following an indirect pathway ($S_1 \rightarrow T_2 \rightarrow T_1$). The present work beautifully demonstrates the role of spin-vibronic coupling in explaining an exotic phenomenon like vibrational coherence transfer in a complex molecule.

Acknowledgement

P. K. thanks the Council of Scientific and Industrial Research (CSIR) for granting him the Junior Research Fellowship. KR has receoved support from the Research Council of Norway through a Centre of Excellence Grant (Grant No 262695). This work has received support from the Norwegian Supercomputer Program NOTUR (Grant No. NN4654K). The support and resources provided by 'PARAM Shakti Facility' under the National Supercomputing Mission, Government of India at the Indian Institute of Technology, Kharagpur, are gratefully acknowledged by SC.

Supporting Information Available

(1) Separation of the real and imaginary parts of the time-dependent correlation function at finite temperature. (2) Coordinates of the optimized geometries of the Pt-pop complex in the gas and solvent(CH_3CN) phases. (3) Frequencies of the optimized geometries of the Pt-pop complex in the gas and solvent phases. 4) Discussions of the structural parameters. (5) Absorption and emission wavelengths and the nature of associated transition orbitals in the solvent phase at different levels of theory. (6) k_{ISC} for additional normal modes of the Pt-pop complex in the solvent phase.(7) Displacement vectors involved with Pt-Pt stretching modes in the gas phase of the S_1 state. (8) Natural transition orbitals (NTOs) in the gas phase with isovalue 0.02. (9) Nature of the active orbitals and their occupation number. (10) Damping of the real part of the time-dependent correlation function(TDCF) for S_1-T_1, S_1-T_2 and S_1-T_3 pathways in the solvent phase. (11) References.

References

(1) Scholes, G. D. Coherence from Light Harvesting to Chemistry. *J. Phys. Chem. Lett.* **2018**, *9*, 1568–1572.

(2) Sio, A. D.; Nguyen, X. T.; Lienau, C. Signatures of Strong Vibronic Coupling Mediating Coherent Charge Transfer in Two-Dimensional Electronic Spectroscopy:. *Z. Naturforsch. A* **2019**, *74*, 721–737.

(3) Gaynor, J. D.; Sandwisch, J.; Khalil, M. Vibronic coherence evolution in multidimensional ultrafast photochemical processes. *Nat. Commun.* **2019**, *10*, 5621.

(4) Gueye, M.; Manathunga, M.; Agathangelou, D.; Orozco, Y.; Paolino, M.; Fusi, S.; Haacke, S.; Olivucci, M.; Léonard, J. Engineering the vibrational coherence of vision into a synthetic molecular device. *Nat. Commun.* **2018**, *9*, 313.

(5) Nelson, T. R.; Ondarse-Alvarez, D.; Oldani, N.; Rodriguez-Hernandez, B.; Alfonso-Hernandez, L.; Galindo, J. F.; Kleiman, V. D.; Fernandez-Alberti, S.; Roitberg, A. E.; Tretiak, S. Coherent exciton-vibrational dynamics and energy transfer in conjugated organics. *Nat. Commun.* **2018**, *9*, 2316.

(6) Ma, F.; Romero, E.; Jones, M. R.; Novoderezhkin, V. I.; van Grondelle, R. Both electronic and vibrational coherences are involved in primary electron transfer in bacterial reaction center. *Nat. Commun.* **2019**, *10*, 933.

(7) Vlček, A. The life and times of excited states of organometallic and coordination compounds. *Coord. Chem. Rev.* **2000**, *200-202*, 933–978.

(8) Zipp, A. P. The behavior of the tetra-μ-pyrophosphito-diplatinum(II) ion $Pt_2(P_2O_5H_2)_4^{4-}$ and related species. *Coord. Chem. Rev.* **1988**, *84*, 47–83.

(9) Chergui, M. Ultrafast Photophysics of Transition Metal Complexes. *Acc. Chem. Res.* **2015**, *48*, 801–808.

(10) Vlcek, A.; Gray, H. B. Binuclear platinum(II) photochemistry. Rates of hydrogen atom transfer from organometallic hydrides to electronically excited $Pt_2(P_2O_5H_2)_4^{4-}$. *J. Am. Chem. Soc.* **1987**, *109*, 286–287.

(11) Roundhill, D. M.; Gray, H. B.; Che, C. M. Pyrophosphito-bridged diplatinum chemistry. *Acc. Chem. Res.* **1989**, *22*, 55–61.

(12) Monni, R.; Auböck, G.; Kinschel, D.; Aziz-Lange, K. M.; Gray, H. B.; Vlček, A.; Chergui, M. Conservation of vibrational coherence in ultrafast electronic relaxation: The case of diplatinum complexes in solution. *Chem. Phys. Lett.* **2017**, *683*, 112–120.

(13) Monni, R.; Capano, G.; Auböck, G.; Gray, H. B.; Vlček, A.; Tavernelli, I.; Chergui, M. Vibrational coherence transfer in the ultrafast intersystem crossing of a diplatinum complex in solution. *Proc. Natl. Acad. Sci.* **2018**, *115*, E6396–E6403.

(14) Durrell, A. C.; Keller, G. E.; Lam, Y.-C.; Sýkora, J.; Vlček, A.; Gray, H. B. Structural Control of $^1A_{2u}$-to-$^3A_{2u}$ Intersystem Crossing in Diplatinum(II,II) Complexes. *J. Am. Chem. Soc.* **2012**, *134*, 14201–14207.

(15) Mewes, L.; Ingle, R. A.; Megow, S.; Böhnke, H.; Baranoff, E.; Temps, F.; Chergui, M. Ultrafast Intersystem Crossing and Structural Dynamics of $[Pt(ppy)(\mu\text{-}^tBu_2pz)]_2$. *Inorg. Chem.* **2020**, *59*, 14643–14653.

(16) Valentine, A. J. S.; Radler, J. J.; Mills, A.; Kim, P.; Castellano, F. N.; Chen, L. X.; Li, X. Resolving the ultrafast intersystem crossing in a bimetallic platinum complex. *J. Chem. Phys.* **2019**, *151*, 114303.

(17) van der Veen, R. M.; Cannizzo, A.; van Mourik, F.; Vlček, A.; Chergui, M. Vibrational Relaxation and Intersystem Crossing of Binuclear Metal Complexes in Solution. *J. Am. Chem. Soc.* **2011**, *133*, 305–315.

(18) Záliš, S.; Lam, Y.-C.; Gray, H. B.; Vlček, A. Spin–Orbit TDDFT Electronic Structure of Diplatinum(II,II) Complexes. *Inorg. Chem.* **2015**, *54*, 3491–3500.

(19) Levi, G.; Pápai, M.; Henriksen, N. E.; Dohn, A. O.; Møller, K. B. Solution Structure and

Ultrafast Vibrational Relaxation of the PtPOP Complex Revealed by ΔSCF-QM/MM Direct Dynamics Simulations. *J. Phys. Chem. C* **2018**, *122*, 7100–7119.

(20) Christensen, M.; Haldrup, K.; Bechgaard, K.; Feidenhans'l, R.; Kong, Q.; Cammarata, M.; Russo, M. L.; Wulff, M.; Harrit, N.; Nielsen, M. M. Time-Resolved X-ray Scattering of an Electronically Excited State in Solution. Structure of the $^3A_{2u}$ State of Tetrakis-μ-pyrophosphitodiplatinate(II). *J. Am. Chem. Soc.* **2009**, *131*, 502–508.

(21) Kim, C. D.; Pillet, S.; Wu, G.; Fullagar, W. K.; Coppens, P. Excited-state structure by time-resolved X-ray diffraction. *Acta Crystallogr. A* **2002**, *58*, 133–137.

(22) Ozawa, Y.; Terashima, M.; Mitsumi, M.; Toriumi, K.; Yasuda, N.; Uekusa, H.; Ohashi, Y. Photoexcited Crystallography of Diplatinum Complex by Multiple-exposure IP Method. *Chem. Lett.* **2003**, *32*, 62–63.

(23) Yasuda, N.; Uekusa, H.; Ohashi, Y. X-ray Analysis of Excited-State Structures of the Diplatinum Complex Anions in Five Crystals with Different Cations. *Bull. Chem. Soc. Jpn.* **2004**, *77*, 933–944.

(24) van der Veen, R. M.; Kas, J. J.; Milne, C. J.; Pham, V.-T.; Nahhas, A. E.; Lima, F. A.; Vithanage, D. A.; Rehr, J. J.; Abela, R.; Chergui, M. L-edge XANES analysis of photoexcited metal complexes in solution. *Phys. Chem. Chem. Phys.* **2010**, *12*, 5551–5561.

(25) van der Veen, R. M.; Milne, C. J.; El Nahhas, A.; Lima, F. A.; Pham, V.-T.; Best, J.; Weinstein, J. A.; Borca, C. N.; Abela, R.; Bressler, C. et al. Structural Determination of a Photochemically Active Diplatinum Molecule by Time-Resolved EXAFS Spectroscopy. *Angew. Chem. Int. Ed.* **2009**, *48*, 2711–2714.

(26) Stiegman, A. E.; Miskowski, V. M.; Gray, H. B. Metal-metal excited-state emission from binuclear platinum(III) complexes. *J. Am. Chem. Soc.* **1986**, *108*, 2781–2782.

(27) Stiegman, A. E.; Rice, S. F.; Gray, H. B.; Miskowski, V. M. Electronic spectroscopy of d_8-d_8 diplatinum complexes. $^1A_{2u}$ ($d\sigma^* \rightarrow p\sigma$), ^3E_u (d_{xz},$d_{yz} \rightarrow p\sigma$), and $^{3,1}B_{2u}$ ($d\sigma^* \rightarrow d_{x^2-y^2}$) excited states of tetrakis(diphosphonato)diplatinate(4-), $Pt_2(P_2O_5H_2)_4^{4-}$. *Inorg. Chem.* **1987**, *26*, 1112–1116.

(28) Gellene, G. I.; Roundhill, D. M. Computational Studies on the Isomeric Structures in the Pyrophosphito Bridged Diplatinum(II) Complex, Platinum Pop. *J. Phys. Chem. A* **2002**, *106*, 7617–7620.

(29) Pan, Q.-J.; Fu, H.-G.; Yu, H.-T.; Zhang, H.-X. Theoretical Insight into Electronic Structures and Spectroscopic Properties of $[Pt_2(pop)_4]^{4-}$, $[Pt_2(pcp)_4]^{4-}$, and Related Derivatives (pop = $P_2O_5H_2^{2-}$ and pcp = $P_2O_4CH_4^{2-}$). *Inorg. Chem.* **2006**, *45*, 8729–8735.

(30) Novozhilova, I. V.; Volkov, A. V.; Coppens, P. Theoretical Analysis of the Triplet Excited State of the $[Pt_2(H_2P_2O_5)_4]^{4-}$ Ion and Comparison with Time-Resolved X-ray and Spectroscopic Results. *J. Am. Chem. Soc.* **2003**, *125*, 1079–1087.

(31) Chaaban, M.; Zhou, C.; Lin, H.; Chyi, B.; Ma, B. Platinum(ii) binuclear complexes: molecular structures, photophysical properties, and applications. *J. Mater. Chem. C* **2019**, *7*, 5910–5924.

(32) Kubo, R.; Toyozawa, Y. The Method of Generating Function Applied to Radiative and Non-Radiative Transitions of a Trapped Electron in a Crystal. *Prog. Theor. Phys.* **1954**, *12*, 805–806.

(33) Etinski, M.; Tatchen, J.; Marian, C. Time-dependent approaches for the calculation of intersystem crossing rates. *J. Chem. Phys.* **2011**, *134*, 154105.

(34) Banerjee, S.; Baiardi, A.; Bloino, J.; Barone, V. Temperature Dependence of Radiative and Nonradiative Rates from Time-Dependent Correlation Function Methods. *J. Chem. Theory Comput.* **2016**, *12*, 774–786.

(35) Baiardi, A.; Bloino, J.; Barone, V. General Time Dependent Approach to Vibronic Spectroscopy Including Franck–Condon, Herzberg–Teller, and Duschinsky Effects. *J. Chem. Theory Comput.* **2013**, *9*, 4097–4115.

(36) Peng, Q.; Niu, Y.; Shi, Q.; Gao, X.; Shuai, Z. Correlation Function Formalism for Triplet Excited State Decay: Combined Spin–Orbit and Nonadiabatic Couplings. *J. Chem. Theory Comput.* **2013**, *9*, 1132–1143.

(37) Tatchen, J.; Gilka, N.; Marian, C. M. Intersystem crossing driven by vibronic spin–orbit coupling: a case study on psoralen. *Phys. Chem. Chem. Phys.* **2007**, *9*, 5209–5221.

(38) Etinski, M.; Rai-Constapel, V.; Marian, C. Time-dependent approach to spin-vibronic coupling: Implementation and assessment. *J. Chem. Phys.* **2014**, *140*, 114104.

(39) Rodriguez-Serrano, A.; Rai-Constapel, V.; Daza, M. C.; Doerr, M.; Marian, C. M. Internal heavy atom effects in phenothiazinium dyes: enhancement of intersystem crossing via vibronic spin–orbit coupling. *Phys. Chem. Chem. Phys.* **2015**, *17*, 11350–11358.

(40) Penfold, T. J.; Gindensperger, E.; Daniel, C.; Marian, C. M. Spin-Vibronic Mechanism for Intersystem Crossing. *Chem. Rev.* **2018**, *118*, 6975–7025.

(41) Frisch, M. J.; Trucks, G. W.; Schlegel, H. B.; Scuseria, G. E.; Robb, M. A.; Cheeseman, J. R.; Scalmani, G.; Barone, V.; Petersson, G. A.; Nakatsuji, H. et al. Gaussian 16 Revision C.01. 2016; Gaussian Inc. Wallingford CT.

(42) Becke, A. Density-functional thermochemistry. III. The role of exact exchange. *J. Chem. Phys.* **1993**, *98*, 5648–5652.

(43) Lee, C.; Yang, W.; Parr, R. Development of the Colle-Salvetti correlation-energy formula into a functional of the electron density. *Phys. Rev. B* **1988**, *37*, 785–789.

(44) Stephens, P.; Devlin, F.; Chabalowski, C.; Frisch, M. Ab Initio Calculation of Vibrational Absorption and Circular Dichroism Spectra Using Density Functional Force Fields. *J. Phys. Chem.* **1994**, *98*, 11623–11627.

(45) Clark, T.; Chandrasekhar, J.; Spitznagel, G. W.; Schleyer, P. V. R. Efficient diffuse function-augmented basis sets for anion calculations. III. The 3-21+G basis set for first-row elements, Li-F. *J. Comput. Chem.* **1983**, *4*, 294–301.

(46) Krishnan, R.; Binkley, J. S.; Seeger, R.; Pople, J. A. Self-consistent molecular orbital methods. XX. A basis set for correlated wave functions. *J. Chem. Phys.* **1980**, *72*, 650–654.

(47) Hay, P.; Jeffrey, W.; R., W. Ab initio effective core potentials for molecular calculations. Potentials for K to Au including the outermost core orbitals. *J. Chem. Phys.* **1985**, *82*, 299–310.

(48) Norman, P.; Jensen, H. J. A. Phosphorescence parameters for platinum (II) organometallic chromophores: A study at the non-collinear four-component Kohn–Sham level of theory. *Chem. Phys. Lett.* **2012**, *531*, 229–235.

(49) Heyd, J.; Scuseria, G. E. Assessment and validation of a screened Coulomb hybrid density functional. *J. Chem. Phys.* **2004**, *120*, 7274–7280.

(50) Adamo, C.; Barone, V. Toward reliable density functional methods without adjustable parameters: The PBE0 model. *J. Chem. Phys.* **1999**, *110*, 6158–6170.

(51) Neese, F. The ORCA program system. *Wiley Interdiscip. Rev. Comput. Mol. Sci.* **2012**, *2*, 73–78.

(52) Neese, F. Software update: the ORCA program system, version 4.0. *Wiley Interdiscip. Rev. Comput. Mol. Sci.* **2018**, *8*, e1327.

(53) Angeli, C.; Cimiraglia, R.; Evangelisti, S.; Leininger, T.; Malrieu, J.-P. Introduction of n-electron valence states for multireference perturbation theory. *J. Chem. Phys.* **2001**, *114*, 10252–10264.

(54) Weigend, F. Hartree–Fock exchange fitting basis sets for H to Rn. *J. Comput. Chem.* **2008**, *29*, 167–175.

(55) Karak, P.; Chakrabarti, S. The influence of spin–orbit coupling, Duschinsky rotation and displacement vector on the rate of intersystem crossing of benzophenone and its fused analog fluorenone: a time dependent correlation function based approach. *Phys. Chem. Chem. Phys.* **2020**, *22*, 24399–24409.

(56) Duschinsky, F. The importance of the electron spectrum in multi atomic molecules. Concerning the Franck-Condon principle. *Acta Physicochim. U.R.S.S.* **1937**, *7*, 551–566.

(57) Etinski, M. The role of Duschinsky rotation in intersystem crossing: A case study of uracil. *J. Serb. Chem. Soc.* **2011**, *76*.

(58) Paul, L.; Moitra, T.; Ruud, K.; Chakrabarti, S. Strong Duschinsky Mixing Induced Breakdown of Kasha's Rule in an Organic Phosphor. *J. Phys. Chem. Lett.* **2019**, *10*, 369–374.

(59) Pokhilko, P.; Krylov, A. I. Quantitative El-Sayed Rules for Many-Body Wave Functions from Spinless Transition Density Matrices. *J. Phys. Chem. Lett.* **2019**, *10*, 4857–4862.